



Synthesis of Zr-doped CeO₂ nanoparticles for photocatalytic degradation of methyl orange and electrochemical properties

K. Haribaaskar¹ · K. S. Yoganand¹ · T. V. Rajendran¹ · M. V. Arularasu²

Received: 29 March 2024 / Revised: 13 June 2024 / Accepted: 10 July 2024

© The Author(s), under exclusive licence to Springer-Verlag GmbH Germany, part of Springer Nature 2024

Abstract

In this work, we have developed template-free growth of Zr-doped CeO₂ and CeO₂ nanoparticles using ultrasonic-assisted techniques for photocatalytic degradation of organic dyes. A variety of techniques such as XRD, FT-IR, FE-SEM, TEM, EDX, and UV–visible spectroscopy were used to study the structural, morphological, elemental, and optical properties of prepared samples. The Zr-doped CeO₂ nanoparticles feature tiny, spherical nanoparticles that range in size from 10 to 20 nm, as shown by the TEM micrographs. The UV–visible absorption spectra of both pure CeO₂ and Zr-doped CeO₂ nanoparticles showed steadily increasing absorption in the visible region. Methyl orange (MO) dye was used to examine the photocatalytic dye degradation capabilities of pure CeO₂ and Zr-doped CeO₂ nanoparticles. The results of this work demonstrate that Zr-doped CeO₂ nanoparticles have a strong MO degradation efficiency (92%) in a time period of 80 min, which is higher than pure CeO₂. The improved photocatalytic activity was achieved due to the Zr-doped CeO₂ nanoparticles having an enlarged light absorption region and an effective electron–hole separation during the photodegradation process. The mechanics of dye degradation have been addressed with reference to the electrochemical impedance spectrum (EIS). These findings exhibit the suitability of the suggested material for real-world uses.

Keywords CeO₂ · Degradation mechanism · Methyl orange · LSV · Impedance spectra

1 Introduction

In recent years, fast-growing industrialization has led to a considerable increase in the use of dyes and pigments to color their products [1–3]. As a result, food and textile industries often discharge large amounts of organic pollutants into the water resulting in continuous destruction of our natural resources [4]. Discharging of these dyes into nearby water bodies is creating environmental pollution due to their high toxicity to humans and marine life; therefore, the elimination

of environmental pollution is one of the widely researched topics [5]. Dye molecules, particularly azo-dyes, are a major class of synthetic organic compounds widely used in various consumer industries such as printing, leather, pharmaceutical, and cosmetics [6, 7]. The contamination of water by MO reduces the water quality and causes genotoxic, mutagenic, and carcinogenic effects on humans and effects on aquatic ecosystems [8]. Therefore, eliminating such dyes from the wastewater is a major task. Various methods have been employed to treat dye-polluted wastewater such as coagulation, filtration, chemical precipitation, and photocatalysis [9, 10]. Among the variety of techniques, semiconductor-based metal oxide photocatalysis is one of the favorable and efficient green techniques and a sustainable and cost-effective method for degrading harmful organic pollutants from wastewater. During photocatalytic degradation, organic pollutants break chemical bonds or decompose dyes into non-toxic chemicals with high elimination efficiency. Therefore, in this work, we chose the photocatalytic method for the degradation of MO dye.

CeO₂ is a rare earth metal oxide semiconductor, which has been widely used for fuel cells, luminescent materials, sensors, and UV blockers and as a catalyst due to its

✉ K. S. Yoganand
yoganand.ks@gmail.com

✉ M. V. Arularasu
arulrs597@gmail.com

¹ Department of Chemistry, SRM Institute of Science and Technology, Ramapuram, Chennai 600089, India

² Sustainable Energy and Environment Research Unit, Center for Global Health Research, Saveetha Medical College and Hospital, Saveetha Institute of Medical and Technical Science, Saveetha University, Chennai 602105, Tamil Nadu, India

versatile physical and chemical properties [11, 12]. CeO₂ has a wide bandgap energy (3.19 eV) and large excitation binding energy; it is a promising photocatalyst for the degradation of organic pollutants [13]. Furthermore, the fast transition between the two oxidation states (Ce(III) and Ce(IV)) generates more oxygen vacancies, which makes CeO₂ a promising material as a photocatalyst and for various applications [14–16]. However, CeO₂ slightly absorbs visible light utilization to separate electron–hole pairs because of the large bandgap during photocatalysis. In order to overcome this problem, CeO₂ is doped with transition and rare earth metals such as Co, Cr, Nb, Zr, Sm, and La, which can enhance the photocatalytic efficiency ascribed to promote the separation of electron–hole pairs, thus facilitating surface reaction [17–20].

In this present work, we report the preparation of pure CeO₂ and Zr-doped CeO₂ nanoparticles by an ultrasonic-assisted method for MO dye. As per our knowledge, this is the first report to synthesize Zr-doped CeO₂ nanoparticles by using an ultrasonic method for the application of photocatalytic degradation of MO dye. These methods were adopted due to the fewer steps involved and environment-friendly method. Various physico-chemical methods such as XRD, FT-IR, FE-SEM, TEM, and UV–visible spectroscopy were used for the confirmation of synthesized nanoparticles; further, the photocatalytic mechanism is also discussed in the manuscript.

2 Experimental section

2.1 Chemical and reagents

Cerium nitrate hexahydrate (Ce(NO₃)₃·6H₂O) (98%), zirconium chloride (ZrCl₂) (99.5%), absolute ethanol (C₂H₆O) (99.8%), ammonium hydroxide (NH₄OH) (95–97%), and methyl orange (MO) (90%) are obtained from Sigma-Aldrich and used as received without further purification.

2.2 Synthesis of CeO₂ and Zr-doped CeO₂ nanoparticles

In a conventional synthesis, 50 mL of deionized water and 15 mL of NH₄OH were used to dissolve 2.9 g of Ce(NO₃)₃·6H₂O and 1.3 g of ZrCl₂ in order to maintain an

acidic pH of around 7. Next, the reaction mixture was subjected to a 3-h ultrasonic probe operation (20 kHz, 500 W, Sonics-VCX 500, Taiwan; 30 s each cycle). The reaction mixture produced an off-white precipitate that was repeatedly cleaned to remove contaminants using distilled water and ethanol. Zr-doped CeO₂ powder was finally obtained by filtering, collecting, and vacuum-drying the precipitate for 3 h at 200 °C. The same process was used to generate pure CeO₂ nanoparticles without the addition of zirconium chloride.

2.3 Characterization techniques

Following the preparation of pure CeO₂ and Zr-doped CeO₂ nanoparticles, experimental methodologies were employed to assess their crystalline structure, surface morphology, elemental analysis, and optical properties which were estimated by various experimental techniques as presented in Table 1.

2.4 Photocatalytic activity

MO in a concentration of 5 mg L⁻¹ was used to evaluate the photocatalytic degradation properties of the prepared samples under visible light irradiation (300 W intensity with 420 nm) at room temperature. Twenty-five milligrams of catalyst was mixed in 50 mL of MO solution and continually stirred for 30 min under a completely dark condition in order to achieve equilibrium between the adsorption and desorption of the dyes as well as the photocatalyst. Then, the solution was collected at equal intermissions from the reaction vessel and immediately centrifuged. The degradation of the dye solution was followed by a UV–visible spectrophotometer in the range of 200–800 nm. In order to investigate the recycling of catalyst experiments, an identical catalyst was charged for four consecutive cycles. After each cycle, the catalyst was dried at 60 °C and cleaned with distilled water to eliminate any remaining dye impurities. A standard three-electrode system was utilized to perform electrochemical impedance spectroscopy (EIS) and linear sweep voltammetry (LSV) characterization. The working electrode was silver/silver chloride (Ag/AgCl), which served as the reference electrode. The counter electrode was a platinum wire that was used with 0.1 KCl electrolyte (CHI6116E electrochemical workstation).

Table 1 Experiment carried out for characterization

S. no	Characterization	Instrument
1	Crystallinity	XRD (Shimadzu XRD 6000)
2	Functional group analysis	FT-IR spectroscopy (JASCO FT/IR-6600 spectrometer)
3	Surface morphology and elemental analysis	FE-SEM with an energy-dispersive spectrometer (HITACHI S-3000N), TEM (Jeol/JEM 2100),
4	Optical absorption	UV–visible analysis (UV–Vis double beam spectrometer, UV-2450)

3 Results and discussions

3.1 XRD analysis

The structural analysis of samples is determined by XRD analysis using a radiation source of $\text{CuK}\alpha$ ($\lambda = 1.5405 \text{ \AA}$). The XRD patterns of Zr-doped and pure CeO_2 nanoparticles are shown in Fig. 1. Both the XRD patterns clearly show high intensity and sharp peaks, which are indicative of the material's crystalline nature. Diffraction peaks were observed at $2\theta = 28.68^\circ$, 33.04° , 47.72° , and 56.52° which can be indexed to (111), (200), (002), and (040) planes, respectively, which represent the cubic phase structure of CeO_2 nanoparticle exactly matched to the previous works of literature (JCPDS No. 89–8436) [16]. No other $\text{ZrO}_2/\text{Zr}(\text{OH})_2$ peak was detected for Zr-doped CeO_2 nanoparticles, representing that the product possesses high purity. However, after the addition of Zr into CeO_2 nanoparticles, the peak position is slightly shifted (negligible peak shift) towards the higher 2θ which confirms the Zr getting incorporated into the CeO_2 nanoparticles because of a very small difference in ionic radius of cerium and zirconium ions. The Scherrer formula [17] can be used to estimate the mean size of pure CeO_2 and Zr-doped CeO_2 nanoparticles by calculating the FWHM (full width at half maximum) of the XRD peak.

$$d = 0.89\lambda/\beta\cos\theta.$$

The (111) plane was used to compute the average crystalline size, and it was discovered that the crystalline sizes of pure CeO_2 and Zr-doped CeO_2 nanoparticles were 23 nm and 18 nm, respectively.

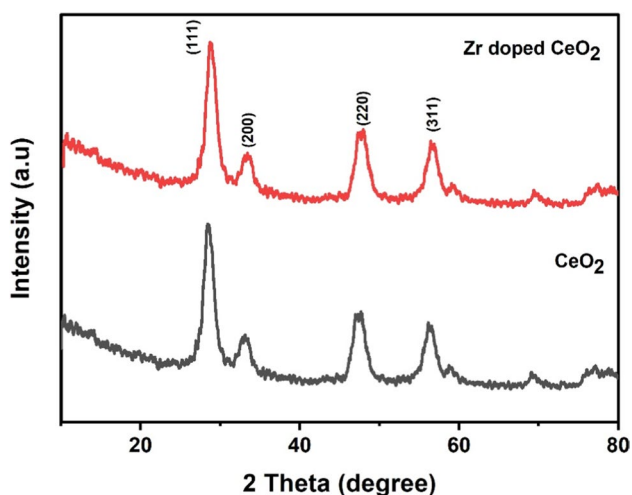


Fig. 1 XRD pattern of CeO_2 nanoparticles and Zr-doped CeO_2 nanoparticles

3.2 FT-IR analysis

In order to confirm the attached functional groups of both samples, the FT-IR spectra were recorded at room temperature. Figure 2 presents the FT-IR spectra of the pure CeO_2 and Zr-doped CeO_2 nanoparticles. In all the samples, the presence of a predominant and sharpest peak that appeared at 425 cm^{-1} was related to Ce–O bonds which confirms the presence of CeO_2 [17]. Different small bands appeared at 641 cm^{-1} and 746 cm^{-1} representing the functional groups' (Ce–O–Ce) symmetric and asymmetric stretching vibration respectively [21]. Characteristic peaks of 1009 cm^{-1} match to the symmetric stretching mode of the $\text{Ce}^{3+}/\text{Ce}^{4+}$ vibration bonds. The peak band that appeared at 3391 cm^{-1} could be assigned to O–H stretching vibration which is due to the existence of phenol and alcohol groups [22, 23]. The appearance of new peaks in Zr-doped CeO_2 nanoparticles compared to CeO_2 nanoparticles might be associated with the change in bond strength and bond angle of CeO_2 due to the incorporation of Zr into the CeO_2 crystal lattice [24].

3.3 FE-SEM and TEM analysis

The microstructure and morphology of Zr-doped CeO_2 nanoparticles and CeO_2 nanoparticles were examined using FE-SEM analysis. The FE-SEM pictures of the Zr-doped CeO_2 nanoparticles and CeO_2 nanoparticles are displayed in Fig. 3. The CeO_2 nanoparticle sample (Fig. 3a) exhibits a clustered morphology with reduced porosity and packed polygonal forms. The FE-SEM picture of Zr-doped CeO_2 nanoparticles, as displayed in Fig. 3b, indicates the presence of significant porosity with a polygonal cluster shape. Generally, nanoparticle-like morphology and dopant ions may provide greater surface area and more active sites

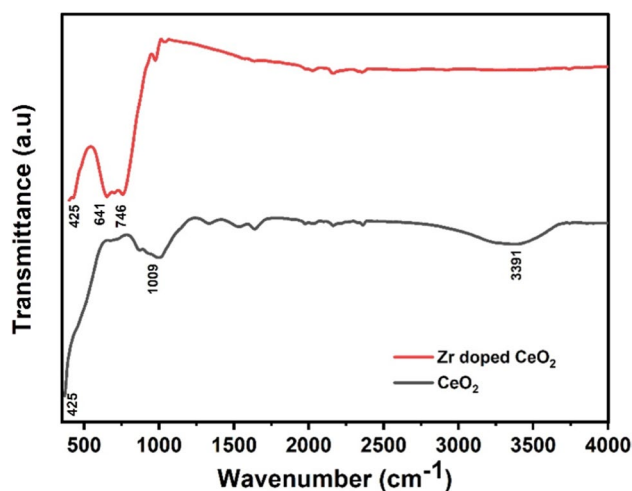


Fig. 2 FT-IR spectra of CeO_2 nanoparticles and Zr-doped CeO_2 nanoparticles

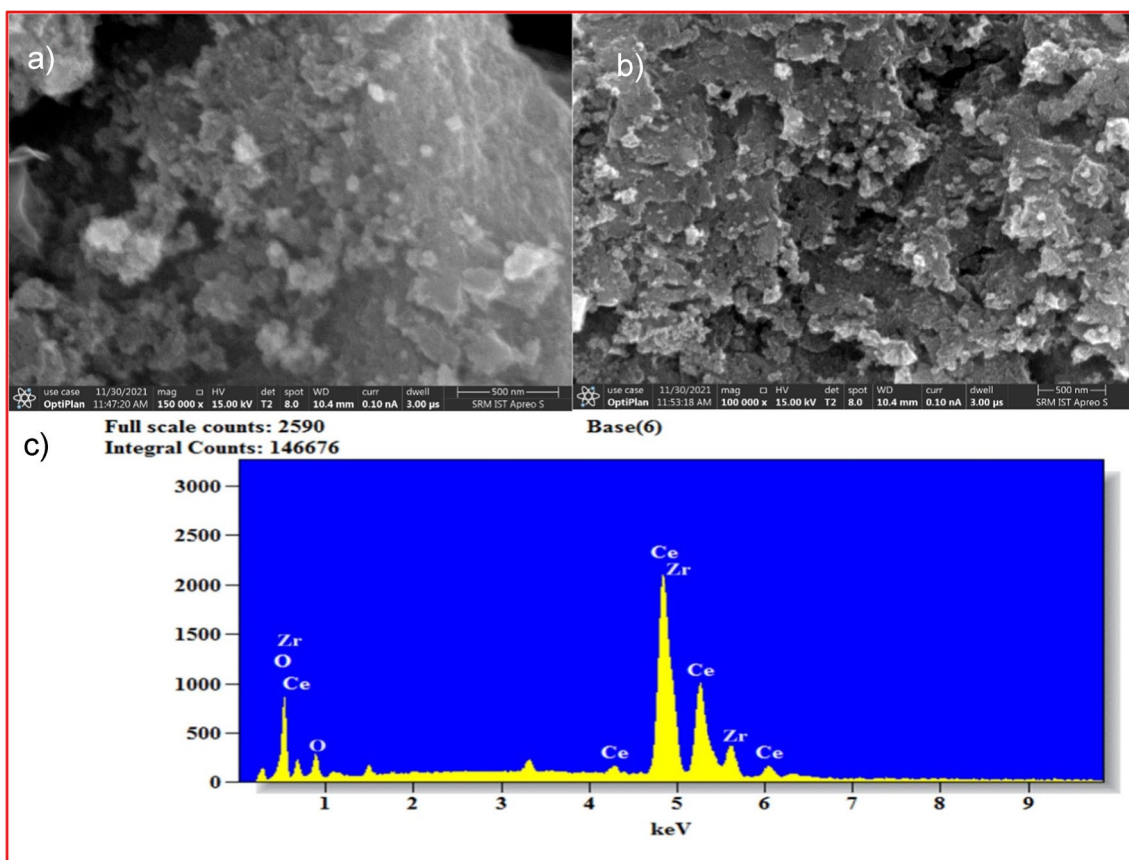
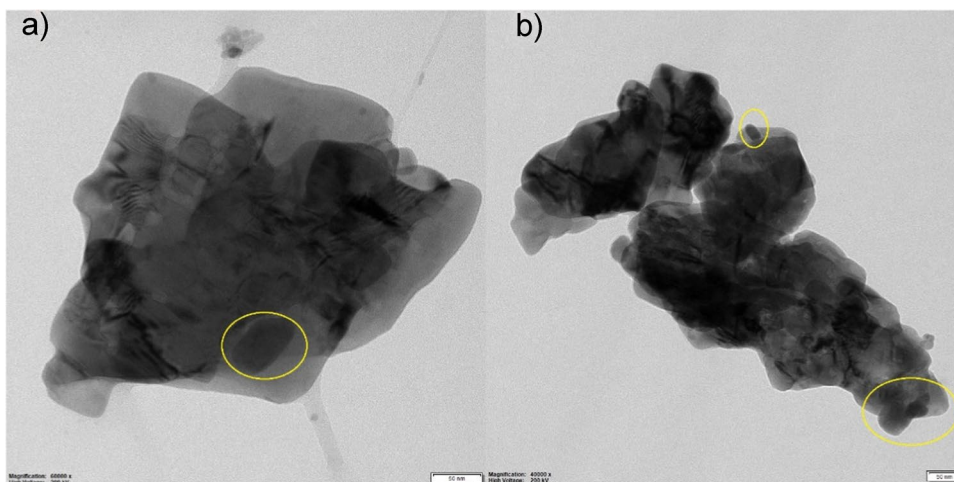


Fig. 3 a) FE-SEM images of CeO_2 nanoparticles, b) Zr-doped CeO_2 nanoparticles, c) EDX spectrum of Zr-doped CeO_2 nanoparticles

on the sample surface which have extreme photocatalytic performance against MO dye. The elemental analysis (qualitative and quantitative) of the prepared samples was examined by EDX spectra (Fig. 3c), which confirmed the samples contained cerium (Ce), oxygen (O), and zirconium (Zr) without any other impurities. A typical TEM image

of CeO_2 nanoparticles and Zr-doped CeO_2 nanoparticles is shown in Fig. 4a and b. From the TEM results, it can be observed the aggregate of particles with less voids and highly crystalline CeO_2 nanoparticles. These available voids facilitate better photocatalytic performance against the MO dye [25, 26].

Fig. 4 a) TEM images of CeO_2 nanoparticles, b) Zr-doped CeO_2 nanoparticles



3.4 UV–Visible spectra

The optical properties of the prepared samples were studied using UV–Vis absorption spectra and are shown in Fig. 5. The absorption edge of both samples appeared at the visible region absorption edge; furthermore, a slight red shift was observed for Zr-doped CeO₂ nanoparticles compared to CeO₂ nanoparticles. The absorption occurs in a visible region for both samples, which can suggest the charge exchange transition of electrons to the infilled Ce orbital from the O valence band. The observed slight red shifting of absorption may be due to the occupancy of the Zr dopant (cation) near the conduction band edge of CeO₂. The observed bandgap values for CeO₂ nanoparticles and Zr-doped CeO₂ nanoparticles are 3 eV and 2.85 eV, respectively. The optical bandgap has been reduced for Zr-doped CeO₂ nanoparticles due to plasmon resonance band. Factors such as the shape and small size of particles influenced the plasmon resonance band formation [27].

Fig. 5 a) UV–visible spectra and b) bandgap of CeO₂ nanoparticles and Zr-doped CeO₂ nanoparticles

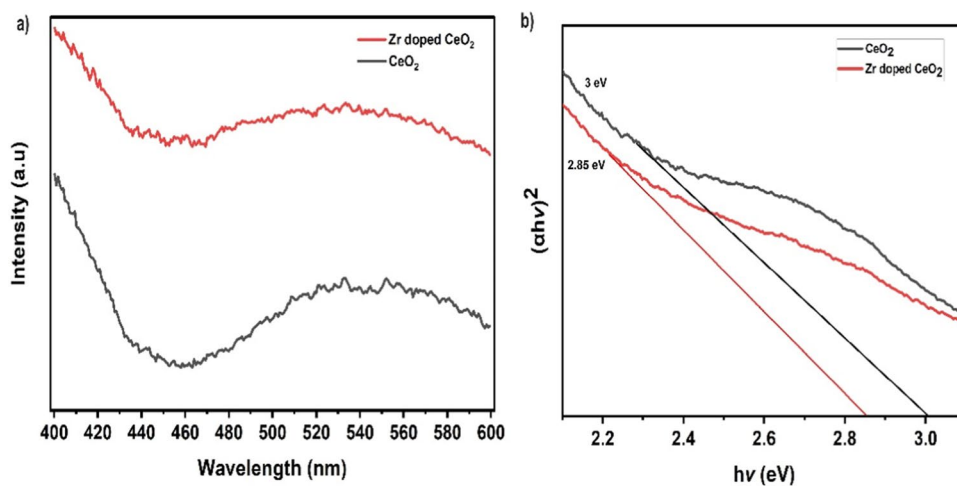
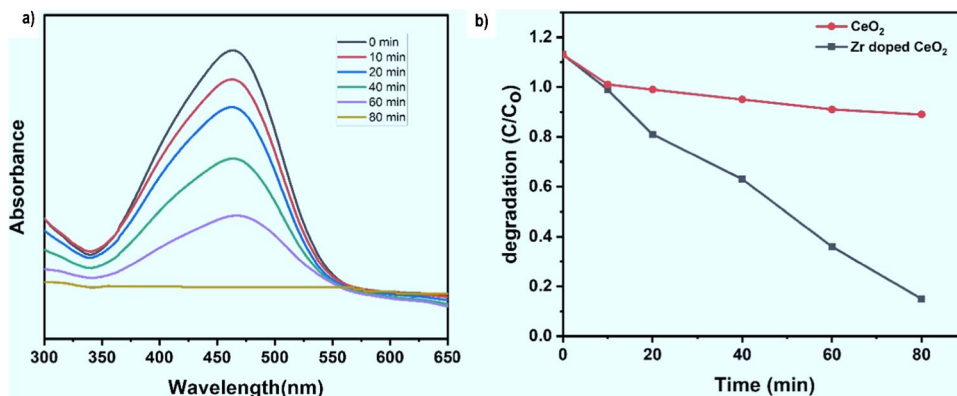


Fig. 6 a) Variation in the absorption spectra of MO on Zr-doped CeO₂ nanoparticles, b) photodegradation activity of CeO₂ and Zr-doped CeO₂ nanoparticles



4 Photocatalytic activity

The effectiveness of CeO₂ nanoparticles and Zr-doped CeO₂ nanoparticles in photocatalytic dye degradation of MO solution under visible light irradiation was used to assess their photocatalytic performance. Using Zr-doped CeO₂ nanoparticles, the complete MO dye photodegradation was stopped after 80 min, as shown in Fig. 6a. It is evident that as the degradation process progressed, the distinctive absorption peak at 464 nm increasingly shrank. Equation 1 is utilized to determine the photocatalytic degradation efficiency of Zr-doped CeO₂ nanoparticles.

$$\eta = \frac{-\ln(C_0 - C_t)}{C_0} \times 100\% \quad (1)$$

C_0 and C_t represent the concentration of MO molecule at the initial stage and at any time “t” min. The degradation process performed by using CeO₂ nanoparticles and Zr-doped CeO₂ nanoparticles catalyst and blank experiment shows the different degradation rates of 92% and 78%, respectively (Fig. 6b). The enhancement in the photocatalytic activity of Zr-doped CeO₂ nanoparticles may be

due to several factors: (i) morphology modification during incorporation of Zr ion CeO_2 nanoparticles; (ii) Zr-dopant ions which can act as charge carrier trap points in the host lattice bandgap and inhabitation of the electron–hole recombination. For comparison, the calculated photocatalytic dye degradation efficiencies of Zr-doped CeO_2 nanoparticles against MO dye are compared with previous literature listed in Table 2 [28–33]. From the tabulated values prepared, Zr-doped CeO_2 nanoparticles are one of the efficient materials for the degradation of MO dye.

4.1 Photocatalytic reusability

A catalyst's reusability is a critical indicator of its practical application. MO photodegradation cycle experiments were conducted to investigate its reusability; it reveals that after four photocatalytic cycles (1st (92%), 2nd (91%), 3rd (89%), and 4th (88.%)), MO degradation efficiency only changed 3.9% over Zr-doped CeO_2 nanoparticles (Fig. 7). The finding that the photocatalytic activity was not greatly reduced indicates that the durability of the Zr-doped CeO_2 sample was not severely impacted by the MO photodegradation process.

4.2 Photocatalytic mechanism of Zr-doped CeO_2

On the outer layer of metal nanoparticles illuminated by visible light, electrons (e^-) in Zr-doped CeO_2 , holes (h^+) are produced in the valence band (VB) as electrons are driven from the VB to the CB [34–36]. The photocatalytic activity is enhanced when CB-stimulated electrons are present in Zr-doped CeO_2 , whereas electron–hole pair recombination rates are reduced. Peroxide radical anions ($\bullet\text{O}_2^-$) are created by the CB electron's reaction towards the dissolved oxygen molecules, while hydroxyl radicals ($\bullet\text{OH}$) are created by the interaction of holes and OH^- ions. The MO dye breaks down and releases CO_2 and H_2O when it is near species of $\bullet\text{OH}$ and $\bullet\text{O}_2^-$. Further carrier charge separation was confirmed by the EIS and LSV method.

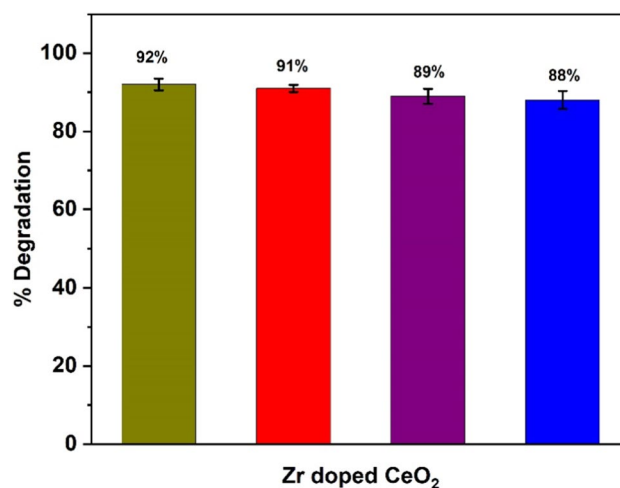


Fig. 7 Reusable performance for the degradation of MO dye using Zr-doped CeO_2 photocatalyst

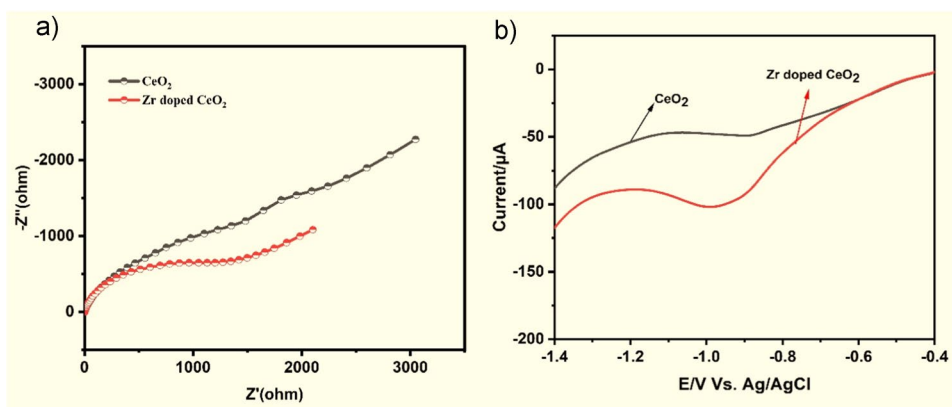
4.3 Electrochemical properties

Electrochemical impedance (EIS) and linear sweep voltammetry (LSV) were performed to explore the charge-transport properties of the photocatalyst. As shown in Fig. 8a, the interfacial charge-transfer properties of pure CeO_2 nanoparticles and Zr-doped CeO_2 nanoparticle photocatalyst-modified electrodes are investigated by the EIS measurement. Both photocatalyst-modified electrode EIS plots have semicircular arcs. The arc area of the semicircle in the EIS plot is equal to the resistance of the interface layer arising at the electrode surface; it can be seen that Zr-doped CeO_2 nanoparticle photocatalyst-modified electrodes show a smaller semicircle arc which corresponds to the lower charge transfer resistance and effective separation of photo-induced electron – holes as well as faster electron transfer so high conductivity of the photocatalyst [37, 38] compare than pure CeO_2 . A semicircle with the smallest arc of Zr-doped CeO_2 nanoparticles indicating doping of Zr ion can greatly accelerate the charge transfer rate of Zr-doped CeO_2

Table 2 Comparison of the other commercial photocatalyst efficiency against different dyes with Zr-doped CeO_2 photocatalyst efficiency

S. no	Photocatalyst (amount of photocatalyst)	Dyes (volume)	Intensity of light	Dye degradation time (min)	Dye degradation efficiency (%)	Ref
1	ZnO nanoparticles (50 mg)	Methyl orange (100 mL)	UV light	180	80	[28]
2	Activated carbon-doped CeO_2 (20 mg)	Crystal violet (60 mL)	Halogen lamp (72 W)	135	97.9	[29]
3	Pd-doped TiO_2 (10 mg)	Methyl orange (20 mL)	Mercury lamp (100 W)	180	75	[30]
4	Carbon-encapsulated V_2O_5 (15 mg)	Crystal violet (60 mL)	Halogen lamp (72 W)	105	98	[31]
5	Co_3O_4 nano arc (5 mg)	Rhodamine B (50 mL)	Solar simulator (150 W)	180	97	[32]
6	La-doped CeO_2 (5 mL)	Methyl blue (60 mL)	Xenon lamp (150 W)	30	70	[33]
7	Present work (25 mg)	Methyl orange (50 mL)	Visible light (300 W)	80	92	-

Fig. 8 a) EIS spectra and b) LSV images of CeO₂ nanoparticles and Zr-doped CeO₂ nanoparticles



sample and can be used as an excellent photocatalyst for the dye degradation process.

Meanwhile, the linear sweep voltammetry (LSV) was carried out to confirm the photogenerated charge carrier separation efficiency of the photocatalyst. As displayed in Fig. 8b, it can be seen that the Zr-doped CeO₂ nanoparticle modified electrode enhanced photocurrent density more than the pure CeO₂ nanoparticle modified electrode. Therefore, the above results confirmed that the Zr-doped CeO₂ interface that can effectively separate electron–hole pairs resulting from the dopant of Zr ion into CeO₂ can promote the photocatalytic degradation efficiency of Zr-doped CeO₂ nanoparticles.

5 Conclusions

In conclusion, methyl orange was broken down using an ultrasonic synthesis of pure CeO₂ and Zr-doped CeO₂ nanoparticles. By using XRD, FT-IR, FE-SEM, TEM, and UV–visible spectroscopy, the structural, morphological, and optical characterizations of pure CeO₂ and Zr-doped CeO₂ nanoparticles were verified. In the visible region, the bandgap values of pure CeO₂ and Zr-doped CeO₂ nanoparticles were found to be 3 eV and 2.85 eV, respectively, based on their cubic face structure. Zr-doped CeO₂ nanoparticles indicated the highest photodegradation efficiency of 92% of MO during 80 min of visible light irradiation over the pure CeO₂. Investigated Zr-doped CeO₂ nanoparticle photocatalyst was suitable for practical application in MO treatment as it showed higher activity even after 4th cycle. Overall, this ultrasonic-assisted method affords a very efficient route for the preparation of stable and effective Zr-doped CeO₂ nanoparticle catalyst for the MO dye from various industrial effluents.

Author contribution K. Haribaaskar: conceptualization; methodology; writing—original draft; investigation; software; methodology. K. S. Yoganand: investigation; writing—reviewing and editing. T. V.

Rajendran: conceptualization; methodology; investigation; software. M. V. Arularasu: methodology; funding acquiring; writing—rewriting draft.

Data availability The datasets generated and analyzed during the current study are available from the corresponding author on reasonable request.

Declarations

Ethical approval There is no animal testing done in the present work.

Competing interests The authors declare no competing interests.

References

- González-Pedroza MG, Benítez AR, Navarro-Marchal SA, Martínez-Martínez E, Marchal JA, Boulaiz H, Morales-Luckie RA (2023) Biogeneration of silver nanoparticles from *Cuphea procumbens* for biomedical and environmental applications. *Sci Rep* 13:790
- Li P, Guo M, Wang Q, Li Z, Wang C, Chen N, Wang CC, Wan C, Chen S (2019) Controllable synthesis of cerium zirconium oxide nanocomposites and their application for photocatalytic degradation of sulfonamides. *Appl Catal B* 259:118107
- Tavan M, Hanachi P, Hossein Mirjalili M, Dashtbani-Roozbehani A (2023) Comparative assessment of the biological activity of the green synthesized silver nanoparticles and aqueous leaf extract of *Perilla frutescens* (L.). *Sci Rep* 13:6391
- Wang L, Li Z, Chen J, Huang Y, Zhang H, Qiu H (2019) Enhanced photocatalytic degradation of methyl orange by porous graphene/ZnO nanocomposite. *Environ Pollut* 249:801–811
- Trandafilovic LV, Jovanovic DJ, Zhang X, Ptainka S, Dramicanin MD (2017) Enhanced photocatalytic degradation of methylene blue and methyl orange by ZnO: Eu nanoparticles. *Appl Catal B-Environ* 230:740
- Yang R, Wu Z, Yang Y, Li Y, Zhang L, Yu B (2021) Understanding the origin of synergistic catalytic activities for ZnO based sonophotocatalytic degradation of methyl orange. *J Taiwan Inst Chem Eng* 119:128–135
- Trandafilović LV, Jovanović DJ, Zhang X, Ptaśńska S, Dramićanin MD (2017) Enhanced photocatalytic degradation of methylene blue and methyl orange by ZnO: Eu nanoparticles. *Appl Catal B* 203:740–752

8. Le Minh Tri N, Trung DQ, Van Thuan D, Dieu Cam NT, Al Tahtamouni T, Pham TD, Duc DS, Thanh Tung MH, Van Ha H, Anh Thu NH, Trang HT (2020) *Int J Hydrog Energy* 45:18186–18194
9. Heidari Z, Alizadeh R, Ebadi A, Oturan N, Oturan MA (2020) Efficient photocatalytic degradation of furosemide by a novel sonoprecipitated ZnO over ion exchanged clinoptilolite nanorods. *Sep Purif Technol* 242:116800
10. Jajakrishnan C, Sheeja SR, Duraimurugan J, Prabhu S, Rameh R, Suresh Kumar G, Mahadevan P, Shkir M (2022) Photoelectrochemical properties and photocatalytic degradation of methyl orange dye by different ZnO nanostructure. *J Mater Sci: Mater Electron*. 33:9732–9742
11. Naidi SN, Harunsani MH, Tan AL, Khan MM (2022) Structural, morphological and optical studies of CeO₂ nanoparticles synthesized using aqueous leaf extract of *Pometia pinnata*. *BioNanoSci* 12:393–404
12. Khan MA, Siddique MA, Sajid M, Karim S, Ali MU, Abid R, Bokhari SA (2023) A comparative study of green and chemical cerium oxide nanoparticles (CeO₂-NPs): from synthesis, characterization, and electrochemical analysis to multifaceted biomedical applications. *BioNanoSci*. 13:667–685
13. Toloman D, Popa A, Bianca Sonher R, Bortnic R, Florin Marinca T, Perhaita L, Filip M, Mesaros A (2024) Enhancing the photocatalytic activity and luminescent properties of rare-earth-doped CeO₂ nanoparticles. *Applied Sciences* 14:522
14. Ankita A, Chahal S, Singh S, Kumar S, Kumar P (2024) Europium-doped cerium oxide nanoparticles: investigating oxygen vacancies and their role in enhanced photocatalytic and magnetic properties. *Environ Sci Pollut Res* 31:1276–1287
15. George J, Palanisamy K, Kulandaivel SP, Saravanana P, Peedika DM, Rajagopalan K, Kaliyannan MK (2023) Impact of cerium oxide nanoparticles on survivability and reproduction of earthworm *Eudrilus eugeniae* and its compost quality. *BioNanoSci* 13:1911–1921
16. Saravanakumar K, Mymoon Ramjan M, Suresh P, Muthuraj V (2016) Fabrication of highly efficient visible light driven Ag/CeO₂ photocatalyst for degradation of organic pollutants. *J Alloys Compd* 664:149–160
17. Senthilkumar RP, Bhuvaneshwari V, Ranjithkumar R, Sathiyavimal S, Malayaman V, Chandarshekar B (2017) Synthesis, characterization and antibacterial activity of hybrid chitosan–cerium oxide nanoparticles: as a bionanomaterials. *Int J Biol Macromol* 104:746–752
18. Qi Y, Ye J, Zhang S, Tian Q, Xu N, Tian P, Ning G (2019) *J Alloys Compd* 782:780–788
19. Rangaswamy A, Sudarsanam P, Reddy BM (2015) Rare earth metal doped CeO₂-based catalytic materials for diesel soot oxidation at lower temperatures. *J Rare Earths* 33:1162–1169
20. Jayakumar G, Irudayaraj AA, Raj AD et al (2022) A study on the photocatalytic efficiency of Ni²⁺, Cd²⁺, and Nb⁵⁺ doped CeO₂ nanoparticles. *Biomass Conv Bioref*. <https://doi.org/10.1007/s13399-022-03543-5>
21. Reddy Yadav LS, Lingaraju K, Daruka Prasad B, Kavitha C, Banuprakash G, Nagaraju G (2017) Synthesis of CeO₂ nanoparticles: photocatalytic and antibacterial activities. *Eur Phys J Plus* 132:239
22. Miri A, Sarani M (2018) Characterization and cytotoxic activity of CeO₂ nanoparticles. *Ceram Int* 44(11):12642
23. Abdelfatah AM, Fawzy M, Eltaweil AS, El-Khouly ME (2021) Green synthesis of nano-zero-valent iron using *Ricinus communis* seeds extract: characterization and application in the treatment of methylene blue-polluted water. *ACS Omega* 6:25397
24. Roza L, Febrianti Y, Iwan S, Fauzia V (2020) The role of cobalt doping on the photocatalytic activity enhancement of ZnO nanorods under UV light irradiation. *Surfaces and Interfaces* 18:100435
25. Maria Magdalane C, Kaviyarasu K, Arularasu MV, Kanimozhi K, Ramalingam G (2019) Structural and morphological properties of Co₃O₄ nanostructures: investigation of low temperature oxidation for photocatalytic application for waste water treatment. *Surf Interfaces* 17:100369
26. Wang D, Zhao L, Ma H, Zhang H (2017) Liang-Hong Guo, Quantitative analysis of reactive oxygen species photogenerated on metal oxide nanoparticles and their bacteria toxicity: the role of superoxide radicals. *Environ Sci Technol* 51:10137
27. Arularasu MV, Harb M, Vignesh R, Rajendran TV, Sundaram R (2020) PVDF/ZnO hybrid nanocomposite applied as a resistive humidity sensor. *Surfaces and Interfaces* 21:100780
28. Sendhil M, Sindhuja K, Arularasu MV (2021) Green synthesis of zinc oxide nanoparticles from *Camellia sinensis*: organic dye degradation and antibacterial activity. *Inorg Chem Commun* 134:108956
29. Sekar S, Bathula C, Rabani I, Woo Lee J, Hyun Lee S, Soo Seo Y, Lee S (2022) *Ultrason Sonochem* 90:106177
30. Nguyen CH, Fu C-C, Juang R-S (2018) Degradation of methylene blue and methyl orange by palladium-doped TiO₂ photocatalysis for water reuse: efficiency and degradation pathways. *J Cleaner Prod* 202:413
31. Seka S, Rabani I, Bathula C, Kumar S, Govindaraju S, Yun K, Soo Seo Y, Young Kim D, Lee S (2022) Graphitic carbon-encapsulated V₂O₅ nanocomposites as a superb photocatalyst for crystal violet degradation. *Environ Res* 205:112201
32. Prakash N, Balaji R, Govindaraju S, Pinky Steffi A, Santhanalakshmi N, Mohanraj K, Selvarajan E, Chandrasekar N, Samuel MS (2022) Influence of 2D template-assisted (SBA-15) metal oxide Co₃O₄ for pseudocapacitive and dye degradation application. *Environ Res* 204:112383
33. Chatterjee M, Mondal M, Sukul T, Mal S, Ghosh K, Das S, Kumar Pradhan S (2023) Superior photocatalytic performance and photo disinfection of bacteria of solvothermally synthesized mesoporous La-doped CeO₂ under simulated visible light irradiation for wastewater treatment. *J Alloys Compd* 942:169135
34. Chen DD, Yi XH, Ling L, Wang CC, Wang P (2023) Photocatalytic Cr(VI) sequestration and photo-Fenton bisphenol A decomposition over white light responsive PANI/MIL-88A(Fe). *Appl Organomet Chem* 34(9):e5795
35. Zhang ZC, Wang FX, Wang F, Wang CC, Wang P (2023) Efficient atrazine degradation via photoactivated SR-AOP over S-BUC-21(Fe): the formation and contribution of different reactive oxygen species. *Sep Purif Technol* 307:122864
36. Mondal Bibhutoh A, Debkumar Mukherjee A (2015) Room-temperature synthesis of air stable cobalt nanoparticles and their use as catalyst for methyl orange dye degradation. *Colloids Surf A: Physicochem Eng Asp* 482:248–257
37. Balu S, Velmurugan S, Palanisamy S, Shih-Wen C, Velusamy V, Yang Thomas C.K., El-Shafey El-Said I (2019) Synthesis of α -Fe₂O₃ decorated g-C₃N₄/ZnO ternary Z-scheme photocatalyst for degradation of tartrazine dye in aqueous media. *J Taiwan Inst Chem Eng* 99:258–267
38. Faria K (2021) Naqvi, Kaseed Anwar, and Saba Beg, Ex situ method for photoreduction of the cadmium ion from terbium-loaded bismuth vanadium oxide, *ACS. Omega* 6:31716–31726

Publisher's Note Springer Nature remains neutral with regard to jurisdictional claims in published maps and institutional affiliations.

Springer Nature or its licensor (e.g. a society or other partner) holds exclusive rights to this article under a publishing agreement with the author(s) or other rightsholder(s); author self-archiving of the accepted manuscript version of this article is solely governed by the terms of such publishing agreement and applicable law.